



# THE UNIVERSITY *of* EDINBURGH

## Edinburgh Research Explorer

### Ionic liquid mediated surface micropatterning of polymer blends

**Citation for published version:**

Lasseguette, E, McClements, J, Koutsos, V, Schaefer, T & Ferrari, M-C 2018, 'Ionic liquid mediated surface micropatterning of polymer blends' Journal of Applied Polymer Science, vol. 135, no. 14, 46109. DOI: 10.1002/app.46109

**Digital Object Identifier (DOI):**

[10.1002/app.46109](https://doi.org/10.1002/app.46109)

**Link:**

[Link to publication record in Edinburgh Research Explorer](#)

**Document Version:**

Peer reviewed version

**Published In:**

Journal of Applied Polymer Science

**General rights**

Copyright for the publications made accessible via the Edinburgh Research Explorer is retained by the author(s) and / or other copyright owners and it is a condition of accessing these publications that users recognise and abide by the legal requirements associated with these rights.

**Take down policy**

The University of Edinburgh has made every reasonable effort to ensure that Edinburgh Research Explorer content complies with UK legislation. If you believe that the public display of this file breaches copyright please contact [openaccess@ed.ac.uk](mailto:openaccess@ed.ac.uk) providing details, and we will remove access to the work immediately and investigate your claim.



# Ionic liquid mediated surface micropatterning of polymer blends

Elsa Lasseuguette<sup>a</sup>, Jake McClements<sup>a</sup>, Vasileios Koutsos<sup>a</sup>, Thomas Schäfer<sup>b</sup>, Maria-Chiara Ferrari<sup>a</sup>

<sup>a</sup> School of Engineering, Institute for Materials and Processes, The University of Edinburgh, Robert Stevenson Road, Edinburgh EH9 3FB, United Kingdom

<sup>b</sup> Polymat University of the Basque Country, Av. Tolosa 72, 20018 Donostia-San Sebastián, Spain and Ikerbasque, Basque Foundation for Science, Bilbao, Spain

Correspondence to: Elsa Lasseuguette, e.lasseuguette@ed.ac.uk

## ABSTRACT

A polymer of intrinsic porosity (i.e. PIM-1) has been blended with different ionic liquids (ILs) in order to evaluate the effect of the ILs on the microstructure of the polymer blend. [C<sub>8</sub>MIM][Cl], [BMIM][Dca], [BMPyr][Dca] and [BMIM][Tf<sub>2</sub>N] have been selected and were mixed with PIM-1. Polymer blend containing up to 80 wt.% of ILs were prepared by a casting method with chloroform as solvent. SEM images show that during the film formation a structuring of the surface appears depending on the nature and the concentration of ILs, with appearance of well-defined microstructure in the case of [BMIM][Tf<sub>2</sub>N] and [BMIM][Dca]. In the case of [BMIM][Tf<sub>2</sub>N]/PIM-1 film, the lower IL concentration induces the denser film with small micropatterns onto the surface. AFM analysis indicates that the ILs are well dispersed on the surface. XPS, FTIR and water contact angle measurements show that a gradient of IL concentration is observed across the film thickness.

It is demonstrated that ILs are versatile co-solvents for inducing controlled micropatterns in polymer membrane surfaces.

## INTRODUCTION

Surface micropatterning of polymers is of great interest in the (bio)medical field for scaffolding or targeting cell adhesion<sup>1-4</sup>, but also as a means to create bioinspired polymer surfaces with antifouling properties<sup>5, 6</sup>. The challenge in micropatterning consists in providing cost efficient, straightforward and reliable fabrication methods<sup>7</sup>.

Strong interest in polymer patterning is due to their relatively low cost, good mechanical properties, and the possibility of easy chemical or physical modification. The current methods of polymers patterning are based on conventional lithographic methods, nano-imprint lithography, laser scanning, electron beam lithography, direct writing. However, in some cases, such as for high-resolution patterning, they are expensive<sup>7-9</sup>. New methods based on self-assembly polymers, phase separation and/or surface instabilities systems have been developed, and allow to obtain well-defined polymeric patterns with dimensions ranging from a few tens of nm to a few mm<sup>7,10</sup>.

Phase separation occurs for immiscible blends, initiated by the loss of solvent by evaporation<sup>10, 11</sup>. The rapid increase in the viscosity of the film freezes the phase-separated structure in place. This process is very sensitive to a variety of parameters including film thickness<sup>12</sup>, substrate (polymer substrate interactions)<sup>13</sup>, physical and chemical properties of solvent and polymer (such as Hansen solubility parameters, molecular weight, and surface tension)<sup>14</sup>. The different solubilities of polymers in the casting solvent causes demixing of the polymers, leading to different structures with the component of higher solubility being enriched at the film surface<sup>11</sup>. Therefore, by tuning the physical-chemical properties of polymers used in phase separation, several types of patterning could be obtained.

Ionic liquids (ILs) present the advantage to have the possibility to tune easily their physical-chemical properties. ILs are defined as organic salts that melt at or below 100°C, and there are a large number of organic cations and anions that can be combined to form different ionic liquids. Depending of cation/anion combinations, the physical and chemical properties, such as their solubility parameters, can be easily changed<sup>15, 16</sup>. Therefore, ILs can be potentially used to produce regular micropatterns, when they are mixed with polymers, where phase separation occurs. For instance, Halder et al.<sup>17</sup> have developed blend membranes based on ILs ([C<sub>x</sub>mim][Tf<sub>2</sub>N]) and PIM-1. PIM-1, which belongs to the PIM family (Polymers of Intrinsic Microporosity), is a microporous material with a high internal surface area (typically 300–1500 m<sup>2</sup>/g) and highly hydrophobic<sup>18</sup>. During the membrane formation, they have observed a phase separation with the presence of circular/ellipsoidal domains due to the partial insolubility of PIMs within ILs. They noted that these areas changed with increasing content of ionic liquid in the blend and with the length of the alkyl chain in the incorporated ILs. We extended this research by using different types of ILs in order to show their possible use for producing regular micropatterns of different shapes. To our knowledge, no attempts have been reported on using ILs to tune surface patterning polymer.

In this paper, we developed a scalable method of blending polymers and ionic liquids to produce highly regular and reproducible micropatterns, which can be used for biomedical applications (antifouling properties). For that, blend polymers composed of ionic liquids and PIM-1 have been prepared. Their surface and structure properties were analyzed with focus on the effect of ionic liquid nature and content.

## EXPERIMENTAL

### Materials

PIM-1 (Figure1) was kindly provided in powder form by the School of Chemistry, University of Edinburgh, UK (Prof. Neil McKeown).

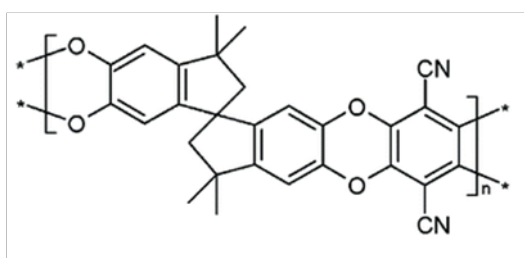


FIGURE 1: Chemical structure of PIM-1.

For this project, four ILs, 1-octyl-3-methylimidazolium chloride, [C<sub>8</sub>MIM][Cl], 1-Butyl-3-Methylimidazolium dicyanamide, [BMIM][DCa], 1-Butyl-1-methyl pyrrolidinium Dicyanamide, [BMPyr][DCa], 1-n-butyl-3-methylimidazolium bis(trifluoromethylsulfonyl)imide, [BMIM][Tf<sub>2</sub>N], named respectively IL1, IL2, IL3 and IL4 were used.

Ionic liquids (Table 1) and chloroform were purchased respectively from Solvionic and VWR and used without purification.

	Ionic liquid	Structure
IL1	1-octyl-3-methylimidazolium chloride [C <sub>8</sub> MIM][Cl]	
IL2	1-Butyl-3-Methylimidazolium dicyanamide [BMIM][DCa]	

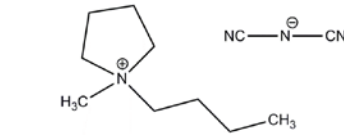
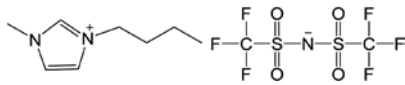
IL3	1-Butyl-1-methyl pyrrolidinium Dicyanamide [BMPyr][DCa]	
IL4	1-n-butyl-3-methylimidazolium bis(trifluoromethylsulfonyl)imide [BMIM][Tf2N]	

TABLE 1: Name and structure of the ionic liquids used in this study.

Nitrogen and carbon dioxide were purchased from BOC and dried before use.

### Hansen solubility parameter

The morphology of the blend polymer will depend on the miscibility of its individual components. There are several ways to predict and explain the miscibility in multiple phase system using thermodynamics, including solubility parameters, lattice theories, and equations-of-state. The so-called Hansen solubility parameters (HSP) have classically been applied to the evaluation of compounds chemical interactions. According to Hansen<sup>19</sup>, the solubility parameter ( $\delta$ ) for a compound is made up of three (non-equally) contributing components. These are: hydrogen bonding force contribution ( $\delta_h$ ), dispersion force contribution ( $\delta_d$ ), and polar force contribution ( $\delta_p$ ). Thus the solubility parameter can be defined by Equation 1.

$$\delta^2 = \delta_h^2 + \delta_d^2 + \delta_p^2 \quad (1)$$

This multi-component system solubility parameter means that each sample can be represented by a fixed point on a ternary plot. The solubility region for a sample can be visualized as a sphere, in a 3D coordinate system with the axes  $\delta_h$ ,  $\delta_p$  and  $\delta_d$ , the centre coordinates of which corresponds to the partial solubility parameters of the sample. These three Hansen parameters can be considered the coordinates of a point in the so-called Hansen space. The closer two points are, the more likely the compounds are to dissolve into each other. Therefore, the affinity between two components 1 and 2 can be defined by the parameter  $R_a$  (Equation 2):

$$R_a^2 = (\delta_{h1} - \delta_{h2})^2 + 4(\delta_{d1} - \delta_{d2})^2 + (\delta_{p1} - \delta_{p2})^2 \quad (2)$$

The smaller the  $R_a$ , the more likely they are to be compatible.

## **Film preparation**

### ***Pristine PIM-1 films***

Pristine PIM-1 films were casted from a filtered 2 wt.% chloroform solution (VWR, UK). The films were dried initially at room temperature for 3 days and then in a vacuum oven at 80° C for 1 day. Films with a final thickness ranging from 60 to 80  $\mu\text{m}$  were obtained (Mitutoyo, Digimatic Disc Micrometer).

### ***PIM-1/IL blend films***

A 2 wt.% PIM-1 solution in chloroform was prepared and stirred for 5 h. Once PIM-1 was fully dissolved, the IL was added and stirred overnight. Then, the solution was filtered through a cellulose filter in order to remove impurities and solid particles, and casted onto a Petri dish. The films were dried initially at room temperature for 3 days and in a vacuum oven at 80° C for 1 day to remove any remaining solvent.

The IL content was varied from 0 wt.% to 80 wt.%. At higher IL content, the film became very brittle.

## **Analysis**

Infrared spectra were recorded using attenuated total reflectance (ATR) mode with Perkin Elmer Frontier FTIR spectrometer in a spectral range of 600-4000  $\text{cm}^{-1}$  with a resolution of 4  $\text{cm}^{-1}$  and an average of 10 scans.

Contact angle measurements and image analysis have been done using a FTA200 Dynamic Contact Angle Analyzer. The measurements were taken at room temperature using distilled water. The measurements were repeated (5 times) on different locations (3 locations) of the samples and averaged. The tangent method was used to calculate the contact angle.

The films have been examined with a Hitachi4700II cold Field Emission Scanning Electron Microscope operating at 5 keV. Before SEM analysis, the samples were sputtered with a thin layer of gold. The images were analysed using ImageJ 1.50i.

Atomic Force Microscopy (AFM) imaging was carried out on a Bruker Multimode/Nanoscope IIIa instrument (Bruker, Santa Barbara, Ca, USA) using two scanners with different scan ranges. A J-scanner was used for larger images which has a lateral range of up to 160  $\mu\text{m}$ , and an E-scanner was used for smaller images with a lateral range of up to 15  $\mu\text{m}$ . Bruker NTESPA cantilevers (aluminium-coated back

side) were employed with a nominal resonant frequency of 300 kHz, and a nominal spring constant of 40 N/m. All imaging was carried out in tapping mode in air. Analysis of the images was performed using Gwyddion (<http://gwyddion.net/>)<sup>20</sup>.

X-ray photoelectron spectra were obtained at the National EPSRC XPS Users' Service (NEXUS) at Newcastle University, an EPSRC Mid-Range Facility, using a K-Alpha (Thermo Scientific, East Grinstead, UK) instrument, with an X-ray Source microfocused monochromatic AlK $\alpha$  (X-ray Energy: 1486.6eV).

## RESULTS AND DISCUSSION

### Structure

Sample film photographs of PIM-1 and PIM-1/IL blend are presented in Figure 2. On these pictures, it can be seen that the addition of ILs induces a change of colour, from bright for the neat PIM-1 film to matt yellow for the blend film. This change in appearance might be attributed to the presence of ionic liquid both within the film polymer as well as on the surface<sup>21</sup>.



FIGURE 2: PIM-1 film (left) / PIM-1/IL blend film 7 wt.% (right).

Moreover, the presence of ILs induces also a change of the structure and surface of the film (Figure 3). The figure 3 shows the surface and cross-section SEM images of a neat PIM-1 film, and PIM-1/IL blend films with 15 wt. % of ionic liquids. The neat PIM-1 film (Figure 3A) appears dense with uniform surface, whereas the blend films present holes onto the top surface and inside the film.

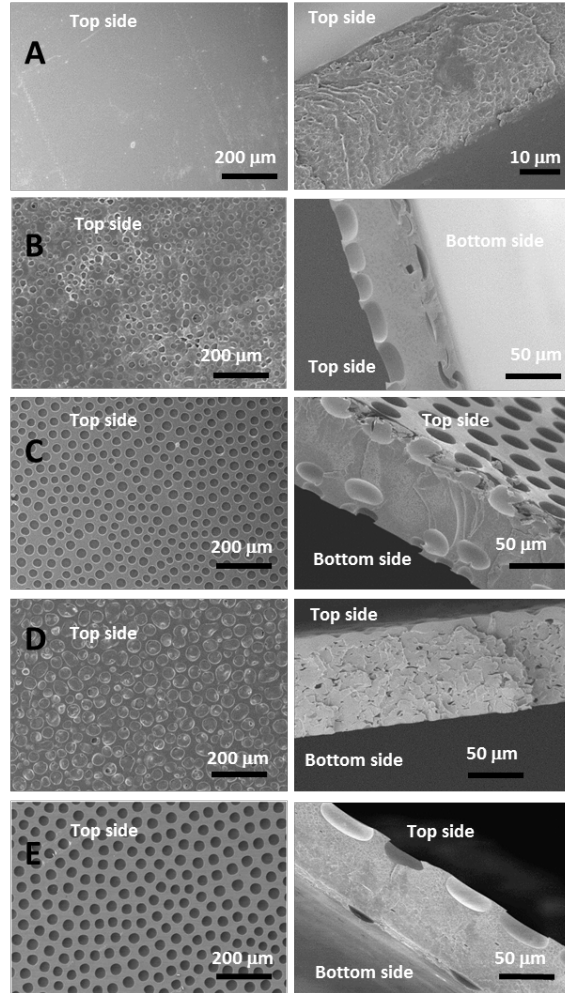


FIGURE 3: SEM images (surface and cross section) of neat PIM-1 (A), PIM-1/IL1 (B), PIM-1/IL2 (C), PIM-1/IL3 (D), PIM-1/IL4 (E) (15 wt.%).

For the films based on IL2 and IL4 (Figure 3C, Figure 3E), a very regular structure, with circular holes on the surface is observed. The holes have a diameter of 40  $\mu\text{m}$  and a depth of 20  $\mu\text{m}$ . They are only present on the top side of the film. For the film based on IL1 (Figure 3B), the holes have less regularity and are smaller. They have diameters between 30  $\mu\text{m}$  and 20  $\mu\text{m}$  and a similar depth of 20  $\mu\text{m}$ . For the blend film based on PIM-1 and IL3 (Figure 3D), the structure is completely different. The film has no holes; the structure is more similar to a roughness of the surface.

This surface structuring might be related to the cation chemical structure of the ionic liquids. Actually, the blend films, PIM-1/IL2 and PIM-1/IL4, which present the same surface structuring, are based on an ionic liquid containing the same cation, namely 1-Butyl-3-Methylimidazolium. For the blend film PIM-1/IL1,



with the slightly different surface, IL1 presents the same cation but with a longer alkyl chain, which induces the non-regularity of the holes and the decrease of their diameter. For PIM-1/IL3 film, the structure is completely different due to the fact that IL3 has a different cation based on a methylpyrrolidinium moiety. These different interactions between PIM-1 and ILs can be explained by the Hansen solubility parameters. IL2 and IL4 have similar Hansen solubility parameters (Table 2) with the same contributions for the hydrogen bonding, polar, and dispersion forces.

	$\delta_h$ [MPa] <sup>1/2</sup>	$\delta_d$ [MPa] <sup>1/2</sup>	$\delta_p$ [MPa] <sup>1/2</sup>	$\delta$ [MPa] <sup>1/2</sup>
IL1	20.7	19.1	20.7	34.9
IL2	10.7	17.6	14.8	25.4
IL3	15.8	15.8	9.8	24.5
IL4	10.7	18.1	14.8	25.7
Chloroform	5.70	17.80	3.10	19.00

TABLE 2: Hansen solubility parameters<sup>22-24</sup>.

Consequently, they present identical chemical interactions with PIM-1 and with chloroform, and thus, a similar behaviour during the film formation. For IL1, the hydrogen contribution is higher than the ones of IL2 and IL4. For IL3, the total Hansen solubility parameter is similar to IL2 and IL4 but the polar contribution is lower, which means that IL3 is less compatible with a polar compound, such as PIM-1.

Halder et al.<sup>17</sup> found the same behavior for blend membranes based on IL4 and PIM1, with the formation of ellipsoidal domains due to the phase separation between ionic liquid and PIM1.

Moreover, for the blend films PIM-1/IL1, PIM-1/IL2, and PIM-1/IL4, the surface structuring occurs only on the top side. On the bottom side, the surface is similar to dense PIM-1 film, without holes. Actually, ILs are miscible in chloroform but only partially miscible with PIM-1. As chloroform evaporates through the film top layer during film formation, it will generate a solubility gradient for ILs across the film thickness, favouring its enrichment where it remains at the final stage which is the top layer.

The impact of IL concentration on the film structure has been studied for the IL4. According the ratio of IL4/PIM-1 in the polymer blend, it is possible to obtain different film structures (Figure 4).

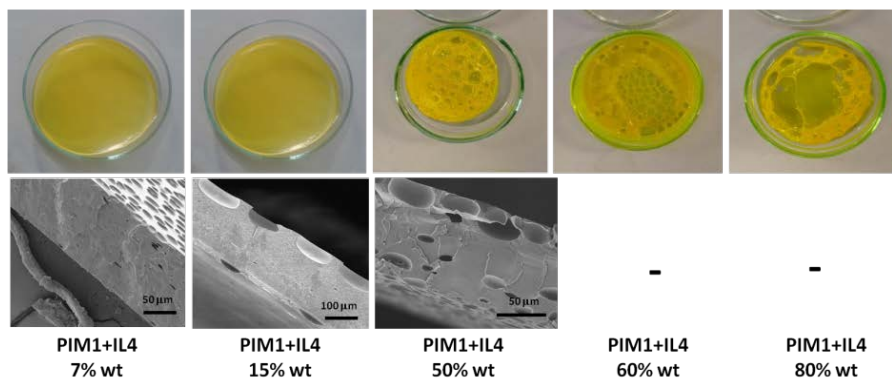


FIGURE 4: SEM cross-section of PIM-1/IL4 at different concentrations.  
*(60 wt.% and 80 wt. % films were too brittle to be analysed).*

With concentration of ionic liquid below 15 wt.%, a dense film with a regular surface structuring has been obtained with holes only on the surface whereas with a high ionic liquid concentration (>50 wt.%), the holes on the surface are larger and the film is porous throughout the thickness. With higher concentration (>60 wt.%), the film became very brittle. The size of the holes increases with the IL4 concentration. For 7 wt.% IL4, the holes on the surface have a diameter of 5  $\mu\text{m}$  whereas for 30 wt.%, the diameter goes up to 60  $\mu\text{m}$ . These holes are induced by the low solubility of PIM-1 with IL4. By looking at the HSP (Figure 5), the IL4 is situated in the same area as the partial solvents of PIM-1, which means low affinity towards PIM-1.

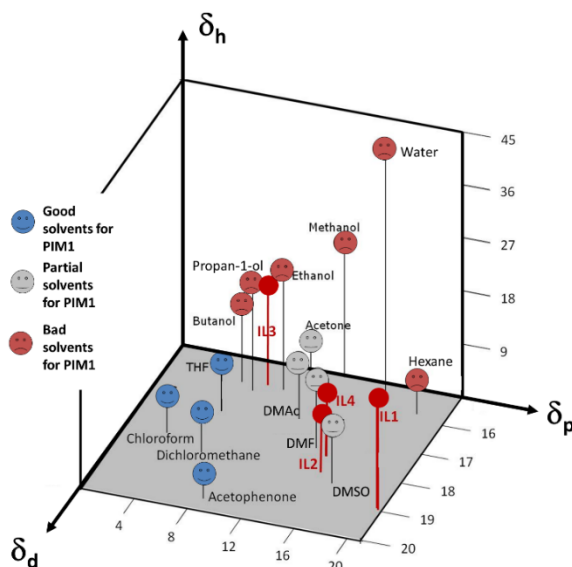


FIGURE 5: Hansen solubility parameters of solvents and ILs<sup>19, 25-27</sup>.

## Surface analysis

The ATR-FTIR spectra of the top/bottom surfaces of the blend films and pristine PIM-1 are presented in figure 6.

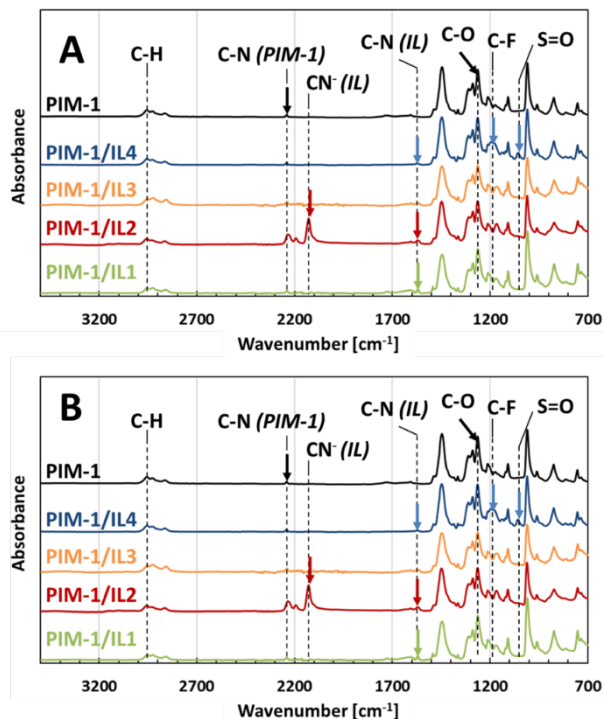


FIGURE 6: ATR-FTIR spectra of PIM-1 and PIM-1/IL blend films top (A) and bottom (B) side.

For the blend films, no absorption peak appears on the ATR-FTIR spectra other than the peaks of pristine PIM-1 and the ILs, respectively. This suggests that no new bonds are present, i.e. no chemical reaction occur between ILs and PIM1. Halder et al.<sup>17</sup> showed similar results on their PIM1/ILs blend membranes, by <sup>1</sup>H NMR characterizations. They did not find new peaks; only peaks from PIM1 and ILs are present on the spectra.

ATR-FTIR peaks corresponding to PIM-1 such as 2240 cm<sup>-1</sup> (CN), 1262 cm<sup>-1</sup> (C-O), are observed on both sides of all the films. The presence of the ILs is confirmed by the absorption peaks at 2018 cm<sup>-1</sup> (C-N<sup>-</sup>, IL2), 1565 cm<sup>-1</sup> (C=N stretch, ILs), 1135 cm<sup>-1</sup> (C-F stretch, IL4), 1049 cm<sup>-1</sup> (S=O bending, IL4). The presence of these peaks is observed on the two sides of the film which suggests the IL is well dispersed on both film surfaces.

For the blend film based on IL3, no peaks corresponding to IL3 were observed such as 2018 cm<sup>-1</sup> which corresponds to its anion CN<sup>-</sup> (dicyanamide). This either means that IL3 is not present on the film or its

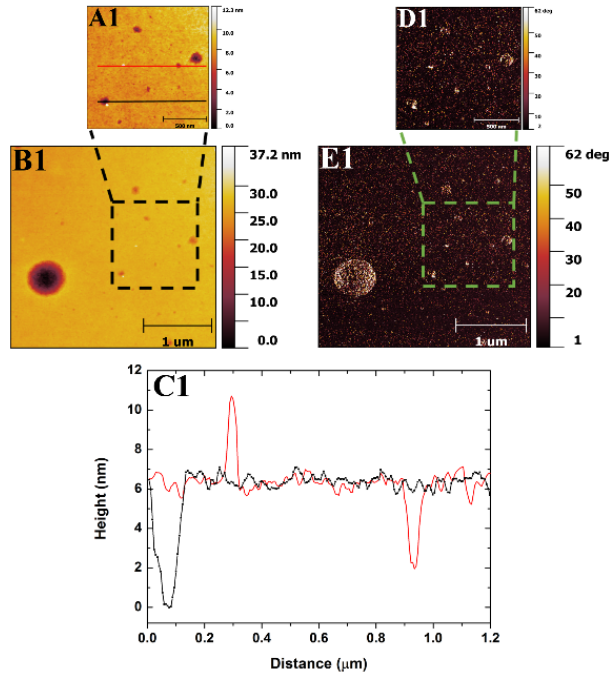
concentration is below the detection limit. In fact, IL3 exhibits a similar HSP as the non-solvents of PIM-1 (Figure 5) evidencing that PIM-1 and IL3 are not miscible. This explains also the different surface structuring obtained for the PIM-1/IL3 blend film and demonstrates the usefulness of the HSP for predicting IL-polymer interactions.

In order to further understand how the incorporation of the ILs determined the polymer morphology, AFM analysis, contact angle measurements and XPS analysis have been performed with the PIM-1/IL4 blends. Atomic force microscopy (AFM) can image surfaces in the nanoscale and provide detailed information about the structure of a surface<sup>28</sup>. AFM images (Figure 7) are presented to show the differences and similarities between the pristine PIM-1 film surface and the PIM-1/IL4 blend film surface. Height and phase images are presented for each surface. Height images show the surface topography of a sample, whereas phase images show contrast related to the viscoelastic and adhesion properties of the materials making up a sample. It is worthwhile noting that the contrast is affected by topography, but can also be used to provide information about differences in chemical composition as there is a strong contribution by the mechanical properties of materials at the sample surface<sup>29-32</sup>.

Figures 7.A1 and 7.B1 show AFM height images for the pristine PIM-1 film surface. The surface is fairly smooth but with a number of distinct attributes; such as very few raised features and several holes in the surface that have a large range of diameters from less than 40 nm up to 500 nm. The majority of these holes have depths less than 5 nm, however, larger ones have depths of up to 25 nm. As the features have small height values, the surface has a relatively low mean surface roughness of 1.34 nm. Figure 7.C1 shows two-line profile scans: two distinct holes are observed on the surface, but it also shows a raised feature with a height of approximately 4 nm. Figures 7.D1 (zoom) and 7.E1 (large area) show two phase images for the pristine PIM-1 film surface. Contrasting colours are associated with variation in the viscoelastic and adhesion properties on the film surface which can be influenced by the surface topography<sup>33</sup>. The phase shift values are from 1° to 62°, and most of the surface appears to have a phase shift value of around 8°. If the differences in the phase shift values were due to different materials, one would expect to observe distinct and well defined areas with different phase shift values on the surface<sup>30, 34</sup>. However, this is not the case, as the small differences in phase shift values only occur at holes in the surface or at raised features. Therefore, this demonstrates that the change in phase shift values are associated with topography alone. The lower phase shift values relate to surfaces with lower elastic moduli<sup>35-37</sup>. Thus, the

pristine PIM-1 film surface appears to be soft. Overall, it appears that on the pristine PIM-1 film surface there is little variation in viscoelastic and adhesion properties. The phase shift differences observed in the images are due to topography effects which suggests that the PIM-1 surface is homogenous as expected.

(1)



(2)

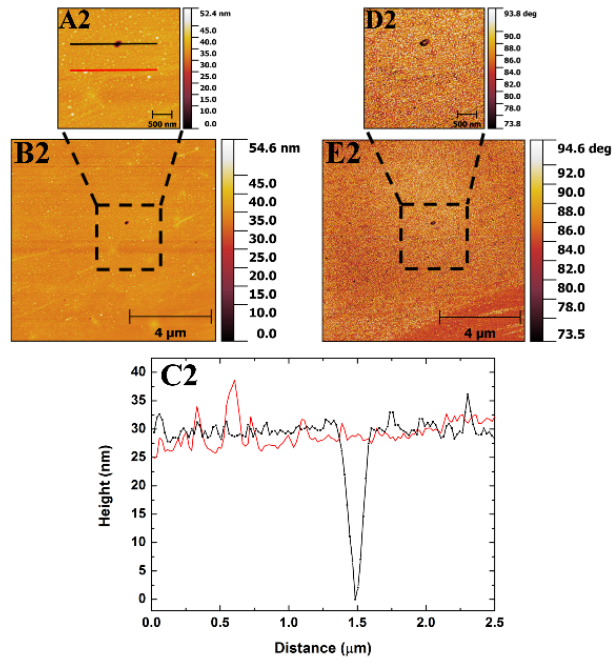


FIGURE 7: A series of AFM images for the pristine PIM-1 film (1) and PIM-1/IL4 (15 wt.%) blend film (2) with corresponding profile plots.

(A), (B) AFM height images for film surface. (C) Line profile scans corresponding to the two horizontal lines on the zoomed image in A. (D), (E) AFM phase images of the film surface. (D) and (E) images were taken simultaneously with the images A and B.

Figures 7.A2 (zoom) and 7.B2 (large area) show AFM height images of the PIM-1/IL4 surface. The AFM images have been taken on the flat surface between the holes. The images show that the surface has many raised features which are generally quite small, with lateral sizes ranging from around 20 nm to 200 nm. The overall mean surface roughness is 1.38 nm which is very similar to the pristine PIM-1 film surface. Although the surface is mostly continuous, there is a small number of circular holes that have diameters ranging from approximately 80 nm up to 290 nm. The depths of these holes are approximately 10 nm for the smaller ones and close to 35 nm for the largest. There is also a small number of straight line features running across the surface, with diameters of  $\sim 62$  nm, and heights of  $\sim 3$  nm. Figure 7.C2 shows two-line profile scans: a large hole is observed on the scan with a depth of around 30 nm, and a number of raised features can also be seen. Figures 7.D2 (zoom) and 7.E2 (large area) show the phase images for the PIM-1/IL4 surface. There appears to be little contrast throughout the surface. The range of phase shift values in Figure 8.E2 are relatively low, spanning from  $73.5^\circ$  to  $94.6^\circ$ , most of the surface is of a similar phase shift value of around  $86^\circ$ . Any changes in the phase shift values on the surface occur at holes or at raised features. This means that once again, the surface is homogenous and phase shift changes are associated with topography<sup>33</sup>. This is exemplified in the bottom right hand corner of the image which shows a smooth area. This smooth area has very little phase shift contrast, showing that the surface topography is causing the differences in phase shift rather than different materials. The phase shift values on this surface are larger than the pristine PIM-1 film; this suggests that when the PIM-1 polymer is mixed with an ionic liquid, the elastic modulus of the material is increased<sup>34-37</sup>. Therefore, it appears that the PIM-1/IL4 sample becomes stiffer but remains homogenous.

Both surfaces have very similar mean surface roughness values, but quite different topographies at the nanoscale. The PIM-1/IL4 surface is stiffer than the pristine PIM-1 film. Both samples appear to be homogeneous, with variations in phase shift being due to surface topography and not materials phase separations.

The contact angle measurements confirm also the presence of IL4 on the two sides of the film. Indeed, the contact angle with water increases up to  $110^\circ$  with the presence of IL4 (Table 3) due to the

hydrophobic nature of IL4<sup>38</sup>, whereas the pristine PIM-1 film has a water contact angle of 77°. However, a difference in contact angle of 10° between the bottom and top side of the film can be noted. This suggests that a concentration gradient exists of the IL across the film thickness, which is in line with the solubility (Figure 5).

Sample	Water contact (°)
PIM-1	77
PIM-IL4 - Top	110
PIM-IL4 - Bottom	100

TABLE 3: Water contact angle measurements.

*The measurements have been taken on the flat surface between the holes.*

This IL4 gradient is also corroborated by XPS analysis. Figure 8 represents the atomic percentage of sulphur and fluorine moieties of the sample. These moieties are only present in the ionic liquid (Table 1). The atomic ratio (F/S) is equal to 3, which is consistent with the chemical formula of IL4. While Figure 8 shows that sulphur and fluorine moieties are present on both sides of the film, it can clearly be seen that there is about half as much of the hydrophobic IL4 on the bottom of the film as on its top surface explaining the difference of water contact angle (Table 3).

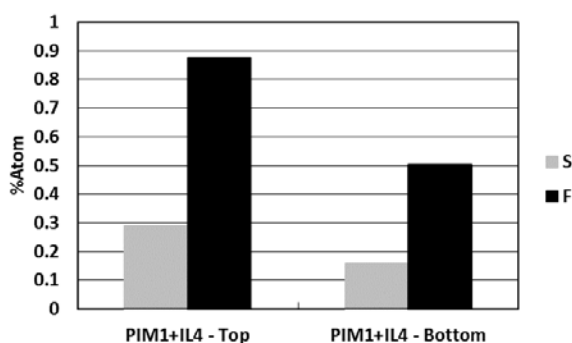


FIGURE 8: S and F content by XPS analysis (%Atom.) PIM-1/IL4 (15 wt.%) polymer blend films.

The incorporation of ILs to PIM-1 allowed the formation of regular hydrophobic micropatterns on the blend surface, which can provide antifouling properties<sup>5</sup>. The hydrophobic character would inhibit the adsorption of proteins, and the surface topography would reduce biofilm formation. However, the biocompatibility and the toxicity of ILs and PIM-1 need to be analyzed.

## CONCLUSIONS

It was shown that ionic liquids can be used as co-solvents for tuning the morphology of blend polymer films. The PIM-1/Ionic liquid blend films developed in this work have shown a surface structuring depending on the concentration and the nature of the ionic liquid. The blend films based on IL with the same cation (IL2 and IL4, 1-Butyl-3-Methylimidazolium) had a regular structuring on the surface with deep holes, whereas the film based on IL3 (with a different cation, Methylpyrrolidinium) had a different surface structuring with smaller holes. Moreover, according to the weight ratio of IL/PIM-1 in the film, it was possible to obtain different film structures. With a low IL concentration (< 15 wt.%), a dense film with a very regular surface structuring has been obtained, whereas with a high IL concentration (>50 wt.%), a porous film has been fabricated. These results suggested that the film structure is due to the insolubility of PIM-1 into ionic liquids. AFM analysis showed that blend polymer films presented a similar surface roughness (~1.35 nm) to PIM-1 films. Both samples appear to be homogeneous. However, the PIM-1/IL4 surface is stiffer than the pristine PIM-1 film. FTIR, XPS analysis and water contact angle measurements showed also the existence of an IL gradient across the thickness.

## ACKNOWLEDGEMENTS

We thank the Moray Endowment Fund Award, the EPSRC and the SOFI CDT (Grant Ref. No. EP/L015536/1) for financial support. X-ray photoelectron spectra were obtained at the National EPSRC XPS Users' Service (NEXUS) at Newcastle University, an EPSRC Mid-Range Facility. T.S. would like to acknowledge funding from ERC (Grant 713641 "ESSENS"), Basque Collaborative Programme Elkartek "LISOL", MINECO (CTQ2013-41113-R, PCIN-2015-240, CTQ2016-80375-P), and DIPC for being hosted.

## REFERENCES

- [1] A. Deglincerti, F. Etoc, M. C. Guerra, I. Martyn, J. Metzger, A. Ruzo, M. Simunovic, S. A. Yoney, A. H. Brivanlou, E. Siggia and A. Warmflash, "Self-organization of human embryonic stem cells on micropatterns", *Nat. Protoc.*, 2016, vol. 11, pp. 2223-2232.
- [2] O. Nedela, P. Slepicka, V. Švorčík, "Surface Modification of Polymer Substrates for Biomedical Applications", *Materials*, 2017, 10, 1115, pp. 1-22.



- [3] Z. Ma, Z. Mao, C. Gao, "Surface modification and property analysis of biomedical polymers used for tissue engineering", *Colloids Surf. B Biointerfaces*, 2007, vol. 60, pp. 137–157.
- [4] J. Ward, R. Bashir, N. Peppas, "Micropatterning of biomedical polymer surfaces by novel UV polymerization techniques", *J. Biomed. Mater. Res.*, 2001, vol. 56, pp. 351-360.
- [5] V. Damodaran, N. S. Murthy, "Bio-inspired strategies for designing antifouling biomaterials", 2016, vol.20-18, pp. 1-11.
- [6] A. M. Brzozowska, F. J. Parra-Velandia, R. Quintana, Z. Xiaoying, S. S. C. Lee, L. Chin-Sing, D. Jańczewski, S. L.-M. Teo and J. G. Vancso, "Biomimicking Micropatterned Surfaces and Their Effect on Marine Biofouling", *Langmuir*, 2014, vol. 30, pp. 9165-9175.
- [7] Z. Nie and E. Kumacheva, "Patterning surfaces with functional polymers", *Nature*, 2008, vol. 7, pp. 277-290.
- [8] O. Lyutakov, J. Tuma, I. Huttel, V. Prajzler, J. Siegel, V. Švorčík, "Polymer surface patterning by laser scanning", *Appl. Phys. B*, 2013, vol. 110, pp. 539–549.
- [9] O. Lyutakov, J. Tuma, J. Siegel, I. Huttel, V. Švorčík, "Nonconventional Method of Polymer Patterning", *Polymer Science*, Dr. Faris Yilmaz (Ed.), InTech, DOI: 10.5772/46143.
- [10] L. Xue, J. Zhang, Y. Han, "Phase separation induced ordered patterns in thin polymer blend films", *Prog. Polym. Sci.*, 2012, vol. 37, pp. 564–594.
- [11] S. Walheim, M. Böltau, J. Mlynek, G. Krausch, U. Steiner, "Structure formation via polymer demixing in spin-cast films", *Macromolecules*, 1997, vol. 30, pp. 4995–5003.
- [12] H. Wang, R.J. Composto, "Wetting and phase separation in polymer blend films: identification of four thickness regimes with distinct morphological pathways", *Interface Sci.*, 2003, vol. 11, pp. 237–248.
- [13] J. Raczowska, J. Rysz, A. Budkowski, J. Lekki, M. Lekka, A. Bernasik, K. Kowalski, P. Czuba, "Surface patterns in solvent-cast polymer blend films analyzed with an integral-geometry approach", *Macromolecules*, 2003, vol.36, pp. 2419–2427.
- [14] S. Walheim, M. Ramstein, U. Steiner, "Morphologies in ternary polymer blends after spin-coating", *Langmuir*, 1999, vol. 15, pp. 4828–4836.
- [15] D. Mecerreyes, "Polymeric ionic liquids: Broadening the properties and applications of polyelectrolytes", *Prog. Polym. Sci.*, 2011, vol. 36, pp. 1629-1648.
- [16] R. Mejri, J. Dias, A. Lopes, S. Hentati, M. Silva, G. Botelho, A. Mão de Ferro, J. Esperança, A. Maceiras, J. Laza, J. Vilas, L. León and S. Lanceros-Mendez, "Effect of ionic liquid anion and cation on the physico-chemical properties of poly(vinylidene fluoride)/ionic liquid blends", *Eur. Polym. J.*, 2005, vol. 71, pp. 304-313.

- [17] K. Halder, M. M. Khan, J. Grünauer, S. Shishatskiy, C. Abetz, V. Filiz and V. Abetz, "Blend Membranes of Ionic Liquid and Polymers of Intrinsic Microporosity with Improved Gas Separation Characteristics", *J. Membr. Sci.*, 2017, vol. 539, pp368-382.
- [18] N. B. McKeown, "Polymers of instrinsic miscroporosity", *ISRN Materials Science*, 2012, pp. 1-16.
- [19] C. Hansen, *Hansen Solubility Parameters: A User's Handbook*, Boca Raton: CRC Press, 2000.
- [20] D. Nečas and P. G. Klapetek, "An Open-Source Software for SPM Data Analysis", *Open Phys*, 2012, vol. 10, pp. 181-188.
- [21] T. Schafer, R. E. Di Paolo, R. Franco and J. G. Crespo, "Elucidating interactions of ionic liquids with polymer films using confocal Raman spectroscopy", *Chem. Commun.*, 2005, pp. 2594-2596.
- [22] L. Hao, P. Li, T. Yang and T. Chung, "Room temperature ionic liquid/ZIF-8 mixed-matrix membranes for natural gas sweetening and post-combustion CO<sub>2</sub> capture", *J. Membr. Sci.*, 2013, vol. 436, pp. 221-231.
- [23] L. Liang, Q. Gan and P. Nancarrow, "Composite ionic liquid and polymer membranes for gas separation at elevated temperatures", *J. Membr. Sci.*, 2014, vol. 450, pp. 407-417.
- [24] D. L. Kim, N. Moreno and S. Pereira Nunes, "Fabrication of polyacrylonitrile hollow fiber membranes from ionic liquid solutions", *Polym. Chem.*, 2016, vol. 7, pp. 113-124.
- [25] P. Weerachanchai, Y. Wong, K. Lim, T. Tan and J. Lee, "Determination of solubility parameters of ionic liquids and ionic liquid/solvent mixtures from intrinsic viscosity", *Chem. Phys. Chem.*, 2014, vol. 15, pp. 3580-3591.
- [26] M. Mora-Pale, L. Meli, T. Doherty, R. Linhardt and J. Dordick, "Room temperature ionic liquids as emerging solvents for the pretreatment of lignocellulosic biomass", *Biotechnol. Bioeng.*, 2011, vol. 108, pp. 1229-1245.
- [27] N. Chaukura and L. Maynard-Atem, "Interaction of a Polymer of Intrinsic Microporosity (PIM-1) with Penetrants", *Am. J. Appl. Chem.*, 2015, vol. 3, pp. 139-146.
- [28] J. Rose, M. Auffan, O. Proux, V. Niviere and Bottero, J. Y. *Encyclopedia of Nanotechnology*, Springer, 2012.
- [29] V. Morris, A. R. Kirby and A. P. Gunning, *Atomic Force Microscopy for Biologists*, second, London: Imperial College Press, 2009.
- [30] D. Raghavan, X. Gu, T. Nguyen, M. VanLandingham and A. Karim, "Mapping Polymer Heterogeneity using atomic force microscopy phase imaging and nanoscale indentation", *Macromolecules*, 2000, vol. 33, pp. 2573-2583.

- [31] R. S. McLean and B. B. Sauer, "Tapping-Mode AFM Studies Using Phase Detection for Resolution of Nanophases in Segmented Polyurethanes and Other Block Copolymers", *Macromolecules*, 1997, vol. 30, pp. 8314-8317.
- [32] M. Kalloudis, E. Glynos, S. Pispas, J. Walker and V. Koutsos, "Thin Films of Poly(isoprene-*b*-ethylene oxide) Diblock Copolymers on Mica: An Atomic Force Microscopy Study", *Langmuir*, 2013, vol. 29, pp. 2339-2349.
- [33] M. Stark, C. Möller, D. J. Müller, and R. Guckenberger, "From Images to Interactions: High-Resolution Phase Imaging in Tapping-Mode Atomic Force Microscopy," *Biophys. J.*, 2001, vol. 80, no. 6, pp. 3009–3018.
- [34] K.-V. Peinemann, V. Abetz, and P. F. W. Simon, "Asymmetric superstructure formed in a block copolymer via phase separation," *Nat. Mater.*, 2007, vol. 6, no. 12, pp. 992–996.
- [35] J. Tamayo and R. García, "Relationship between Phase Shift and Energy Dissipation in Tapping-Mode Scanning Force Microscopy", *Appl. Phys. Lett.*, 1998, vol. 73, pp. 2926-2928.
- [36] B. Bhushan and J. Qi, "Phase Contrast Imaging of Nanocomposites and Molecularly Thick Lubricant Films in Magnetic Media", *Nanotechnology*, 2003, vol. 14, pp. 886-895.
- [37] A. F. Payam, J. R. Ramos and R. Garcia, "Molecular and Nanoscale Compositional Contrast of Soft Matter in Liquid: Interplay between Elastic and Dissipative Interactions", *ACS Nano*, 2012, vol. 6, pp. 4663-4670.
- [38] T. Stockmann and Z. Ding, "Hydrophobicity of room temperature ionic liquids assessed by the Galvani potential difference established at micro liquid/liquid interfaces", *J. Electroanal. Chem.*, 2010, vol. 649, pp. 23-31.